

RSC Advances



This is an *Accepted Manuscript*, which has been through the Royal Society of Chemistry peer review process and has been accepted for publication.

Accepted Manuscripts are published online shortly after acceptance, before technical editing, formatting and proof reading. Using this free service, authors can make their results available to the community, in citable form, before we publish the edited article. This *Accepted Manuscript* will be replaced by the edited, formatted and paginated article as soon as this is available.

You can find more information about *Accepted Manuscripts* in the [Information for Authors](#).

Please note that technical editing may introduce minor changes to the text and/or graphics, which may alter content. The journal's standard [Terms & Conditions](#) and the [Ethical guidelines](#) still apply. In no event shall the Royal Society of Chemistry be held responsible for any errors or omissions in this *Accepted Manuscript* or any consequences arising from the use of any information it contains.

ARTICLE

N-Type KCu_3S_2 Microbelts: Optical, Electrical, and Optoelectronic Properties

Cite this: DOI: 10.1039/x0xx00000x

Chunyan Wu,* Wenjian Wang, Xingang Wang, Jun Xu, Linbao Luo, Shirong Chen, Li Wang, Yongqiang Yu

Received 00th January 2012,

Accepted 00th January 2012

DOI: 10.1039/x0xx00000x

www.rsc.org/

KCu_3S_2 microbelts with lengths up to 80 μm and width of 200-800 nm have been synthesized using a composite-hydroxide mediated (CHM) approach and their optical, electrical and optoelectronic properties were systematically characterized for the first time. As-synthesized KCu_3S_2 microbelts were characterized to be semiconductor with a bandgap of 1.64 eV by UV-vis absorption spectrum and room-temperature PL spectrum. Ultraviolet photoelectron spectroscopy (UPS) and the electrical transport properties of the bottom-gate field-effect transistor (FET) revealed the n-type conduction of the KCu_3S_2 microbelts with a conductivity as high as $\sim 1.85 \times 10^3 \text{ S cm}^{-1}$. A $\text{KCu}_3\text{S}_2/\text{Au}$ Schottky diode was fabricated, which showed a turn-on voltage $\sim 0.3 \text{ V}$, a rectification ratio $\sim 10^2\text{-}10^3$, and an ideality factor 2.1. The diode possessed a photoresponse ratio $I_{\text{light}}/I_{\text{dark}} \sim 50$ and a rapid response time less than 0.5 s. The systematical electrical characterization of KCu_3S_2 microbelts sheds a light on the potential application of KCu_3S_2 as a photovoltaic or optoelectronic material.

1. Introduction

Since the 1990's, quasi one-dimensional (1D) semiconductor micro/nanostructures, especially nanowires and nanobelts, have aroused an increasing interest due to their excellent optical and electronic properties compared to bulk materials and their potential applications as building blocks for functional nanodevices.^{1,2} Till now, various semiconductor nanowires and nanobelts, including group IV elements (Si, Ge, et al), group III-V compounds (GaAs, InP, et al), and group II-VI compounds (ZnS, ZnSe, CdS, CdSe, et al) have been successfully synthesized and used for the fabrication of nanodevices such as photodetectors,³ sensors,⁴ light emission diodes (LEDs),⁵ photoconductive optical switches,⁶ and field effect transistors (FETs).⁷ Copper chalcogenides (CuS , $\text{Cu}_2\text{-xSe}$, et al) quasi 1D nanostructures have also been proved to be potential materials for nanodevices such as solar cells,⁸ non-volatile memories⁹ and gas sensors,¹⁰ recently.

K-Cu-S system is one of the important thiocuprates,¹¹ which are composed of a mono- or two-valent electropositive element (such as alkali metals (Na-Cs), $[\text{NH}_4]^+$, Ca, Tl(I), and Ba), copper and sulphur. It has attracted much research interest since it exists in a variety of composition and has various crystallographic structures as well as unique physical and chemical properties because of the different coordinations copper can adopt, which merits intensive experimental and theoretical studies of transport phenomena of low-dimensional solids.¹² For example, the well-known phases in the K-Cu-S system include KCuS ,¹³ KCu_4S_3 ,^{14,15} $\text{K}_3\text{Cu}_8\text{S}_6$,^{16,17} KCu_3S_2 ,¹⁸ and KCu_7S_4 .^{19,20} The KCuS structure consists of one-dimensional Cu-S chains while KCu_4S_3 adopts a double-layer structure (S-Cu-S-Cu-S). The other three compounds, $\text{K}_3\text{Cu}_8\text{S}_6$, KCu_3S_2 and KCu_7S_4 , can be rewritten as $\text{K}_3\text{Cu}_4\text{S}_2[\text{Cu}_4\text{S}_4]$, $\text{K}_2\text{Cu}_2[\text{Cu}_4\text{S}_4](\equiv 2\text{KCu}_3\text{S}_2)$, and $\text{KCu}_3[\text{Cu}_4\text{S}_4]$, respectively. Each contains Cu_4S_4 columns, in which copper is three-coordinate with respect to sulphur atoms while the

Cu^+ cation outside the Cu_4S_4 column is four-coordinate.²¹ The KCu_4S_3 and $\text{K}_3\text{Cu}_8\text{S}_6$ phases are mixed-valent, and the metallic conductivity arises from holes in the sulphur 3p band as the formal oxidation state of copper in copper chalcogenides is Cu^+ .²² Low temperature phase transitions and resistivity anomalies were observed in the $\text{K}_3\text{Cu}_8\text{S}_6$ and KCu_7S_4 phases, which were reported to originate from an order-disorder transition of the Cu^+ ions in the structure.^{23,24}

However, to the best of our knowledge, only a few researches on the K-Cu-S quasi 1D micro/nanostructures have been reported.²⁵ The reason may be the difficulty to obtain a pure-phase sample with the micro/nanostructures. Herein, KCu_3S_2 microbelts with lengths of tens of micrometers were synthesized, and their optical, electrical and optoelectronic properties were systematically investigated. A $\text{KCu}_3\text{S}_2/\text{Au}$ Schottky diode was fabricated and investigated to show the potential applications of KCu_3S_2 macro/nanobelts in fields such as photovoltaic and optoelectronic devices.

2. Experimental Details

2.1 Synthesis of KCu_3S_2 microbelts

All the reagents (analytical-grade purity) were purchased from Shanghai Chemical Reagents Co. and were used without any further purification.

KCu_3S_2 microbelts were synthesized using a modified composite-hydroxide mediated (CHM) approach in the absence of any organic surfactant with a minor modification.²⁵ A mixture of NaOH (1.29g) and KOH (1.71g) with Na/K atomic ratio of 51.5:48.5 was put into a 50 ml flask, and melted at 165 $^\circ\text{C}$ to form a hydroxide solution. 1 mmol CuCl and 1 mmol $\text{Na}_2\text{S} \cdot 9\text{H}_2\text{O}$ were added into the hydroxide solution with strongly stirring. After keeping the reaction at 165 $^\circ\text{C}$ for 8 h, the flask was taken out and cooled to room temperature

ARTICLE

Journal Name

naturally. The taupe solid products were collected by centrifuging the mixture, and then washed with hot deionized water and absolute ethanol for several times and dried in a vacuum at 60 °C for 4h for further characterization and device fabrication.

2.2 Characterization

As-synthesized products were characterized by X-ray diffraction (XRD, Rigaku D/MAX- γ B, Cu K α radiation, $\lambda = 1.54178\text{\AA}$), scanning electron microscopy (SEM, JSM-6490LV), high-resolution transmission electron microscopy (HRTEM, Philips CM 200 FEG). Composition of the products was detected by the energy-dispersive x-ray spectroscopy (EDS, Oxford INCA, attached to SEM). UV-vis absorption spectrum was performed on a UV-vis spectrometer (CARY 5000). Room-temperature photoluminescence (PL) spectrum was measured using a 532nm He-Cd laser as the excitation source (LABRAM-HR). X-ray photoelectron spectroscopy (XPS, Thermo ESCALAB250, Al K α) and ultraviolet photoelectron spectroscopy (UPS, ULTRA DLD, KRATOS-AXIS-165, Mg K α) were used to determine the interfacial properties and the band offset of the as-synthesized products with high precision.

To assess the electrical properties of the KCu_3S_2 microbelts, bottom-gate field-effect transistors (FETs) based on a single microbelt were constructed. First, the as-synthesized KCu_3S_2 microbelts were dispersed on an HfO_2 (100 nm)/ $\text{p}^+\text{-Si}$ substrate. Then photolithography, thermal deposition and a subsequent lift-off process were utilized to define the In (50 nm) electrodes on the KCu_3S_2 microbelts. The heavily doped Si substrate acted as the global bottom gate in the nanoFETs. In order to construct the $\text{KCu}_3\text{S}_2/\text{Au}$ Schottky junction, the as-synthesized KCu_3S_2 microbelts were dispersed onto a SiO_2 (300 nm)/ $\text{p}^+\text{-Si}$ substrate, then an Au (50 nm) Schottky electrode was fabricated beside the adjacent In (50 nm) electrode through an additional photolithography process. All the electrical measurements were conducted at room temperature with a semiconductor characterization system (Keithley 4200-SCS).

3. Results and Discussions

XRD pattern of the as-synthesized product is shown in Figure 1a. All the diffraction peaks can be well indexed to monoclinic KCu_3S_2 phase (JCPDS card No. 34-0338). No evident impurity peaks from Cu and Cu_2O or other components are observed, indicating that the products are of single phase and high purity. However, the intensity of (001) and (003) peaks are much higher than that reported in the JCPDS card, which implies a dominate crystal plane in the product. Figure 1b presents a typical SEM image of the KCu_3S_2 product, showing a general morphologies of microbelts with lengths up to 80 μm (mostly 10-30 μm), and widths of 200-800 nm. The EDS spectrum (inset of Figure 1b) reveals the sample with an atomic ratio of K:Cu:S = 1:3.25:2.23, which shows a remarkable cation-deficiency when compared to the stoichiometry of KCu_3S_2 . It is noted that the Si peak comes from the Si substrate used for the EDS measurement. Figure 1c and d show the low-resolved TEM and HRTEM images of a KCu_3S_2 microbelt, respectively. The well-defined 2D lattice fringes in the HRTEM image and

the corresponding fast Fourier transform (FFT) pattern (inset of Figure 1d) reveal the single crystallinity of the as-synthesized KCu_3S_2 microbelt. The edge of the microbelt in the HRTEM image is very clear and the interplanar spacings of 0.20 nm and 0.24 nm correspond to the (020) and (003) lattice planes of monoclinic KCu_3S_2 , respectively. Therefore, we can deduce that as-synthesized KCu_3S_2 microbelts grow along the direction [010] and were terminated with crystallographic planes (001) and (100) as shown in the schematic diagram inserted in Figure 1c. What's more, according to ref 25, the microbelts are easily packed to form microslabs with side plane (100) and surface plan (001) due to the opposite surface charge on opposite sides, which, however, contributes to the high intensity of (001) and (003) peaks in the XRD pattern.

Figure 1e shows the survey XPS spectrum of the KCu_3S_2 microbelts. The high-resolution Cu 2p core level XPS is presented in Figure 1f, exhibiting a doublet of Cu 2p $_{3/2}$ peak at 932.2 eV and Cu 2p $_{1/2}$ peak at 952.2 eV. Since the shift of the binding energy is not sensitive enough to determine the Cu valence state, the modified Auger parameter (α') is chosen to determine the chemical state, which is defined as the sum of the kinetic energy of the Auger signal and the binding energy of the photoelectron line. The Auger parameter represents a value of 1849.9 eV from the numerical sum of the Cu 2p $_{3/2}$ line and the Cu LMM line (917.7 eV), suggesting the monovalence state of copper, i.e., Cu(I).^{24, 26}

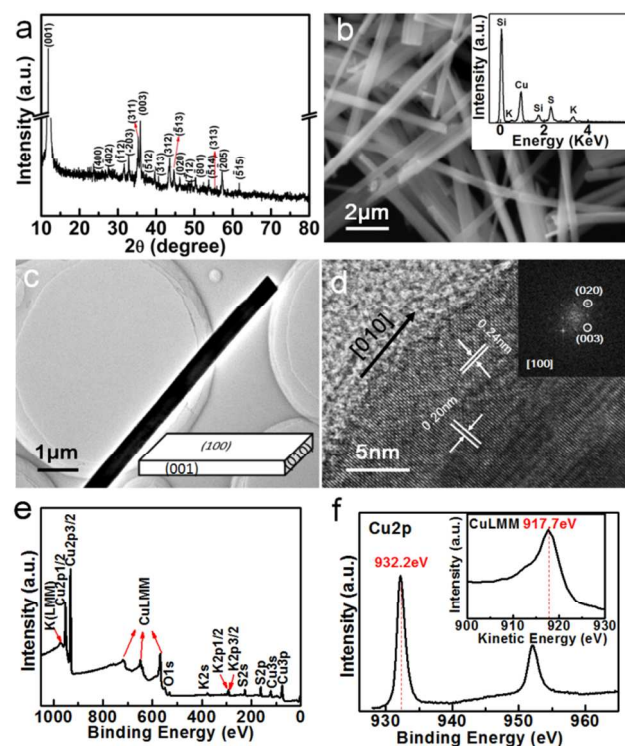


Figure 1. Typical characterizations of the as-synthesized products. (a) XRD pattern, (b) SEM image, inset shows the corresponding EDS spectrum, (c) TEM image, inset shows the schematic diagram of a microbelt, (d) HRTEM image, inset shows the corresponding SAED pattern, and XPS spectrum: (e) survey and (f) Cu 2p XPS spectrum. Inset in (f) shows the CuLMM Auger spectrum.

Figure 2a shows the UV-vis absorption spectrum of the as-synthesized KCu_3S_2 microbelts which increases dramatically when the incident photon energy exceeds 1.6 eV. It exhibits a sharp PL emission peak at 756 nm, as shown in Figure 2b. According to reference 25, this emission corresponds to the near-band-edge (NBE) emission of as-synthesized KCu_3S_2 microbelts, giving a bandgap of 1.64 eV. This is slightly larger than the reported value, which may be caused by the difference between the two products such as unintentional doping or defect arising from the solution-based growth. What's more, the full width at half maximum (FWHM) ($\sim 180\text{meV}$) of the PL peak is relatively larger than that of the well crystallized nanowires,²⁷ which also implies the existence of the doping or defect. Figure 2c-e depict the UPS spectra of the KCu_3S_2 microbelts. The secondary electron onset (SO) on the left side of the spectrum is positioned at 16.76 eV (Figure 2d). By subtracting the SO position from the excitation energy (HeI, 21.22 eV), the work function is calculated to be 4.46 eV. The onset of the valence band maximum (VBM) peak edge is 1.42 eV (Figure 2e), which means that the VBM is located 1.42 eV below the Fermi level and n-type conduction of the KCu_3S_2 microbelts is proved.

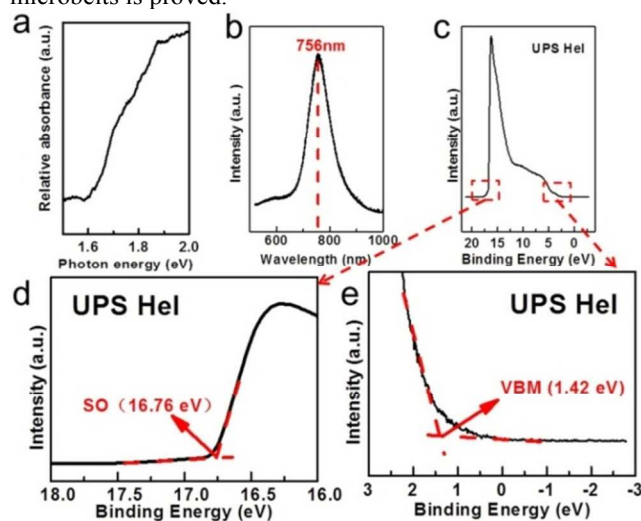


Figure 2. (a) UV-vis absorption spectrum, (b) room temperature PL spectrum ($\lambda_{\text{ex}}=532\text{nm}$), and (c-e) UPS spectra of the as-synthesized KCu_3S_2 microbelts.

Bottom-gate field-effect transistors (FETs) based on the KCu_3S_2 microbelts were fabricated to further study their electrical property and conductivity. Figure 3b plots a typical current versus voltage (I - V) curve of a KCu_3S_2 between two In electrodes in the dark. Ohmic contact of the In electrodes with KCu_3S_2 is revealed by the linear shape of the I - V curve. The conductivity of KCu_3S_2 microbelts is deduced to be about $\sim 1.85 \times 10^3 \text{ S cm}^{-1}$, which is comparable with that of CuS nanotubes.⁸ Figure 3c shows the transport properties of the KCu_3S_2 microbelts. The source-drain current (I_{ds}) versus source-drain voltage (V_{ds}) curves were measured under varied gate voltage V_{g} from -40 to +40 V with a step of 20 V. It is noted that the device exhibits an obvious n-type gating effect, i.e., the conductance increases with increasing V_{g} . This result also reveals the n-type nature of the KCu_3S_2 microbelts. The field-effect electron mobility (μ_n) can be estimated from the channel transconductance (g_m) of the nanoFET according to the

equation $g_m = \frac{dI_{\text{ds}}}{dV_{\text{g}}} = \frac{\mu_n \epsilon_0 \epsilon_{\text{HfO}_2} W V_{\text{ds}}}{hL}$ in the linear regime of the $I_{\text{ds}}-V_{\text{g}}$ curve (inset in Figure 3c), where L is the channel length (55 μm), ϵ_0 is the vacuum dielectric constant, ϵ_{HfO_2} is the dielectric constant of HfO_2 (25), W is the channel width (500 nm), and h is the HfO_2 thickness (100 nm). From the transfer characteristics, g_m is $\sim 87.9 \text{ nS}$ at $V_{\text{ds}} = 0.5 \text{ V}$, resulting in an electron mobility (μ_n) of $\sim 87.4 \text{ cm}^2 \text{ V}^{-1} \text{ s}^{-1}$. Furthermore, the electron concentration (n_n) is deduced to be $\sim 2.81 \times 10^{13} \text{ cm}^{-3}$ through the relation $n_n = \sigma / q\mu_n$, where σ is the conductivity of the microbelt at $V_{\text{g}}=0$, and q is the elementary charge.

Although there is no report on the conduction type of KCu_3S_2 till now, the n-type conduction of the KCu_3S_2 microbelts is unexpected since Cu-based chalcogenide such as Cu_2O ,²⁸ Cu_2S ,²⁹ and Cu_{2-x}Se ³⁰ are all well-known to be cation-deficient p-type semiconductors. The possible reason may be that the KCu_3S_2 microbelts were synthesized in the molten mixed alkali solution. The concentrations of the K^+ and Na^+ cations in the solution were very high. K^+ cations are known to be incorporated into the crystal lattices, forming thiocuprate KCu_3S_2 . And there may be trace Na^+ cations which have also been incorporated, filling the vacancy and serving as the n-type dopant. However, further work is still on the way to clarify it.

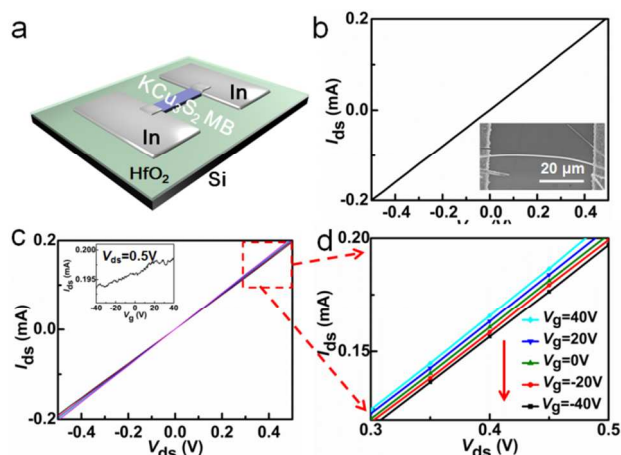


Figure 3. (a) A schematic diagram of the back-gate nanoFET based on the KCu_3S_2 microbelt. (b) The $I_{\text{ds}}-V_{\text{ds}}$ curve of a single KCu_3S_2 microbelt. Inset is the SEM image of a typical nano device based on a single KCu_3S_2 nanobelt. (c) $I_{\text{ds}}-V_{\text{ds}}$ curves measured with V_{g} increasing from -40V to 40V with a step of 20 V. The inset shows the corresponding $I_{\text{ds}}-V_{\text{g}}$ curve at $V_{\text{ds}}=0.5 \text{ V}$. (d) Enlarged view of the dashed rectangle in Figure 3c.

Figure 4a shows a schematic diagram of the $\text{KCu}_3\text{S}_2/\text{Au}$ Schottky diode. The I - V curve measured between the Au and In electrodes shows distinct rectifying characteristics with a turn-on voltage $\sim 0.3 \text{ V}$ and a rectification ratio $\sim 10^2$ - 10^3 (Figure 4b). The ideality factor (n) could be deduced to be ~ 2.1 (inset in Figure 4b), based on the following equation

$$n = \frac{q}{kT} \frac{dV}{d \ln I}$$

where q , k and T represent the electronic charge, Boltzmann's constant, and absolute temperature respectively. This value is larger than that for an ideal diode ($n = 1$). This deviation is likely caused by the enhanced tunnelling current in a nanoscale

ARTICLE

Journal Name

Schottky contact. The ultra-high conductivity of the KCu_3S_2 microbelt is also an important reason, since it can result in a large tunnelling current. Figure 4c shows the typical I - V curves of the $\text{KCu}_3\text{S}_2/\text{Au}$ Schottky diode in dark and upon light illumination (white light from the optical microscopy on the probe station, 3.5 mW cm^{-2}), respectively. A remarkable positive photoresponse can be observed and the time response spectrum (Figure 4d) shows that the device can follow the pulsed optical signal with a response time less than 0.5 s (limited by the speed of manually turning on and off the light) and a response ratio $I_{\text{light}}/I_{\text{dark}} \sim 50$. This result suggests that the electron-hole pairs can be efficiently generated and separated in the $\text{KCu}_3\text{S}_2/\text{Au}$ Schottky diode. Due to the excellent stability and reproducibility, the devices are promising to function as high performance photoswitches.

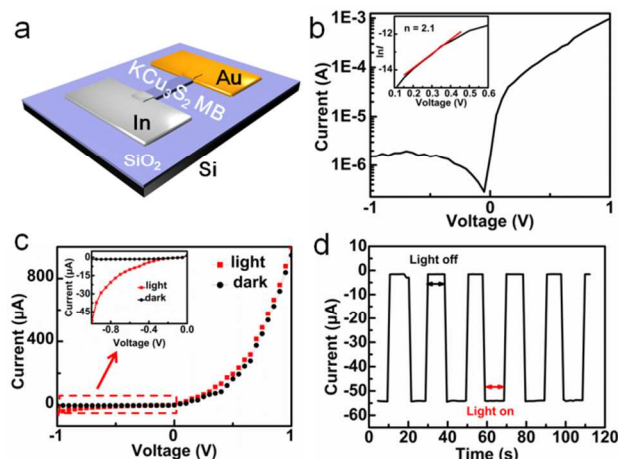


Figure 4. (a) A schematic diagram of the $\text{KCu}_3\text{S}_2/\text{Au}$ Schottky diode nanodevice. (b) I - V curve of the $\text{KCu}_3\text{S}_2/\text{Au}$ Schottky diode measured in dark on a logarithmic scale. Inset presents the plot of $\ln I - V$, showing ideality factor of the $\text{KCu}_3\text{S}_2/\text{Au}$ Schottky diode. (c) I - V curves measured in dark (black curve) and upon light illumination (red curve), respectively. Inset shows the magnification of the zone marked by the rectangle. (d) Time response spectrum of the $\text{KCu}_3\text{S}_2/\text{Au}$ Schottky diode to pulsed light at $V = -1 \text{ V}$.

Energy band diagrams of the $n\text{-KCu}_3\text{S}_2/\text{Au}$ Schottky diode are presented in Figure 5 to interpret the distinct photoresponse characteristics. When there is no bias applied on the diode (Figure 5a), the energy band of the KCu_3S_2 near the metal/semiconductor interface is bended upwards and the electrons are depleted in the near-surface area of KCu_3S_2 . When the diode is reversely biased (Figure 5b), the energy band of KCu_3S_2 will bend upwards further and a larger space-charge region will be formed. Due to the large Schottky barrier at the interface, electrons can hardly drift from KCu_3S_2 into the Au electrode, resulting in a low dark current. When upon light illumination, photo-generated electron-hole pairs in the space-charge region are separated by the electric field in opposite directions. The photo-generated electrons are diffused into

KCu_3S_2 while the photo-generated holes are injected into the Au electrode, leading to a larger photocurrent. As a result, a positive photoresponse is observed for the $\text{KCu}_3\text{S}_2/\text{Au}$ diode.

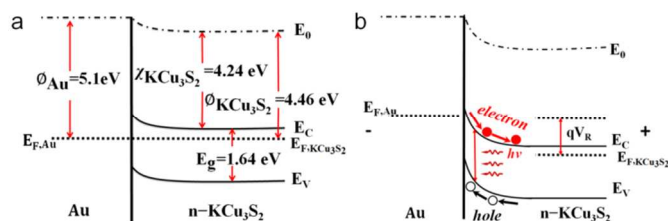


Figure 5. Energy band diagrams of the $n\text{-KCu}_3\text{S}_2/\text{Au}$ Schottky diode at (a) zero bias, and (b) reverse bias. (ϕ_{Au} and $\phi_{\text{KCu}_3\text{S}_2}$ denote the work functions of Au and KCu_3S_2 , respectively. $E_{\text{F,Au}}$ and $E_{\text{F,KCu}_3\text{S}_2}$ denote the Fermi energy level of Au and KCu_3S_2 , respectively. $\chi_{\text{KCu}_3\text{S}_2}$ is the electron affinity of KCu_3S_2 . E_{C} and E_{V} are the conduction band minimum and the valence band maximum of KCu_3S_2 , respectively. E_0 is the vacuum energy level. E_{g} is the band energy of KCu_3S_2 .)

4. Conclusions

In summary, monoclinic KCu_3S_2 microbelts with lengths up to $80 \mu\text{m}$ (mostly $10\text{-}30 \mu\text{m}$), widths of $200\text{-}800 \text{ nm}$ were successfully synthesized using a composite-hydroxide mediated (CHM) approach without using any organic surfactants. UV-vis absorption spectrum and room-temperature PL spectrum proved the microbelts to be semiconductor with a bandgap of 1.64 eV . The n -type conduction of the as-synthesized KCu_3S_2 microbelts was revealed by the UPS spectra and the transport properties of the bottom-gate field-effect transistor (FET), which also exhibits a conductivity $\sim 1.85 \times 10^3 \text{ S cm}^{-1}$ and an electron mobility $\sim 87.4 \text{ cm}^2 \text{ V}^{-1} \text{ s}^{-1}$. Photoresponse property of the $\text{KCu}_3\text{S}_2/\text{Au}$ diode was investigated, showing a turn-on voltage $\sim 0.3 \text{ V}$, a rectification ratio $\sim 10^2\text{-}10^3$, and an ideality factor 2.1. Our work reveals that KCu_3S_2 may be a promising semiconductor and may have potential applications in photovoltaic and optoelectronic devices.

Acknowledgements

This work was supported by the National Natural Science Foundation of China (NSFC, Nos. 20901021, 21101051, 21301044, 61106010), the Natural Science Foundation of Anhui Province of China (No. 1408085MB31), and the Fundamental Research Funds for the Central Universities (Nos. 2013HGJ0195, 2013HGCH0012, and 2014HGCH0013).

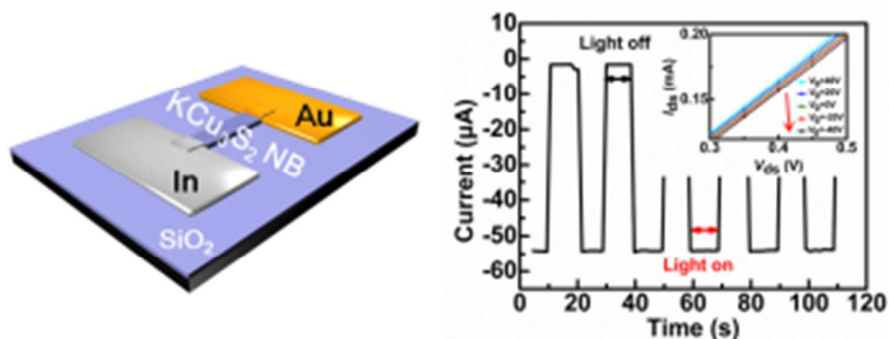
School of Electronic Science and Applied Physics, Hefei University of Technology, Hefei Anhui 230009, People's Republic of China. E-mail: cywu@hfut.edu.cn

Notes and references

- 1 S. Iijima, *Nature*, 1991, **354**, 56.
- 2 C.M. Lieber and L.W. Zhong, *MRS Bull.*, 2007, **32**, 99.
- 3 J. Wang, M.S. Gudiksen, X. Duan, Y. Cui and C. M. Lieber, *Science*, 2001,

- 293, 1455.
- 4 Y. Cui, Q.Q. Wei, H.K. Park and C.M. Lieber, *Science*, 2001, **293**, 1289.
- 5 Y. Huang, X.F. Duan and C.M. Lieber, *Small*, 2005, **1**, 142.
- 6 Q. H. Li, T. Gao and T. H. Wang, *Appl. Phys. Lett.* 2005, **86**, 193109.
- 7 H. Kind, H.Q. Yan, B. Messer, M. Law and P. D. Yang, *Adv. Mater.*, 2002, **14**, 158.
- 8 C.Y. Wu, Z.H. Zhang, Y.L. Wu, P. Lv, B. Nie, L.B. Luo, L. Wang, J.G. Hu and J.S. Jie, *Nanotechnology*, 2013, **24**, 045402.
- 9 C.Y. Wu, Y.L. Wu, W.J. Wang, D. Mao, Y.Q. Yu, L. Wang, J. Xu, J.G. Hu and L.B. Luo, *Appl. Phys. Lett.*, 2013, **103**, 193501.
- 10 J. Xu, W.X. Zhang, Z.H. Yang, S.X. Ding, C.Y. Zeng, L.L. Chen, Q. Wang and S.H. Yang, *Adv. Funct. Mater.*, 2009, **19**, 1759.
- 11 R. Schneider, *J. Pract. Chem.*, 1865, **108**, 16.
- 12 H. Boller, *J. Alloys Compd.*, 2007, **442**, 3.
- 13 G. Savelsberg and H.Z. Schafer, *Z. Naturforsch.*, 1978, **33B**, 711.
- 14 G.V. Vajenine and R. Hoffmann, *Inorg. Chem.*, 1996, **35**, 451.
- 15 B.P. Ghosh, M. Chaudhury and K.J. Nag, *Solid State Chem.*, 1983, **47**, 307.
- 16 W. Rudorff, H.G. Schwarz and M.Z. Walter, *Anorg. Allg. Chem.*, 1952, **269**, 141.
- 17 C.Z. Burschka, *Z. Naturforsch.*, 1979, **34B**, 675.
- 18 C. Burschka and W.Z. Bronger, *Z. Naturforsch.*, 1977, **32B**, 11.
- 19 T. Ohtani, J. Ogura, M. Sakai and Y. Sano, *Solid State Commun.*, 1991, **78**, 913.
- 20 T. Ohtani, J. Ogura, H. Yoshihara and Y.J. Yokota, *Solid State Chem.*, 1995, **115**, 379.
- 21 H. Li, R. Mackay, S.J. Hwu, Y.K. Kuo, M.J. Skove, Y. BYokota and T. Ohtani, *Chem. Mater.*, 1998, **10**, 3172.
- 22 J. Rouxel, *Curr. Sci.*, 1997, **73**, 31.
- 23 M.H. Whangbo and E. Canadell, *Solid State Commun.*, 1992, **81**, 895.
- 24 H. Boller, *J. Alloys Compd.*, 2009, **480**, 131.
- 25 L.Y. Huang, J. Liu, Z.Y. Zuo, H. Liu, D. Liu, J.Y. Wang and R.I. Boughton, *J. Alloys Compd.*, 2010, **507**, 429.
- 26 Y.Q. Yu, Y. Jiang, P. Jiang, Y.G. Zhang, D. Wu, Z.F. Zhu, Q. Liang, S.R. Chen, Y. Zhang and J.S. Jie, *J. Mater. Chem. C*, 2013, **1**, 1238.
- 27 A. Mishra, L.V. Titova, T.B. Hoang, H.E. Jackson, L.M. Smith, J.M. Yarrison-Rice, Y. Kim, H.J. Joyce, Q. Gao, H.H. Tan and C. Jagadish, *Appl. Phys. Lett.*, 2007, **91**, 263104.
- 28 X.M. Liu and Y.C. Zhou, *Appl. Phys. A*, 2005, **81**, 685.
- 29 C.F. Pan, S.M. Niu, Y. Ding, L. Dong, R.M. Yu, Y. Liu, G. Zhu and Z.L. Wang, *Nano Lett.*, 2012, **12**, 3302.
- 30 Y. Zhang, C.G. Hu, C.H. Zheng, Y. Xi and B.Y. Wan, *J. Phys. Chem. C.*, 2010, **114**, 14849.

Graphic Abstract



We report the systematical optical, electrical and optoelectronic characterization of KCu_3S_2 nanobelt, which was proved to be a typical n-type semiconductor with a bandgap ~ 1.64 eV. The Schottky diode based on it shows a stable and quick response to visible light, showing the promise to function as high performance photoswitches.